



ELSEVIER

Spectrochimica Acta Part B 57 (2002) 311–326

SPECTROCHIMICA
ACTA
PART B

www.elsevier.com/locate/sab

Hybrid model for a cylindrical hollow cathode glow discharge and comparison with experiments

N. Baguer*, A. Bogaerts, R. Gijbels

Department of Chemistry, University of Antwerp (UIA), Universiteitsplein 1, B-2610 Wilrijk-Antwerp, Belgium

Received 12 June 2001; accepted 21 November 2001

Abstract

Some of the fundamental characteristics of the hollow cathode glow discharge are presented for different discharge conditions, based on a hybrid Monte Carlo fluid model, and on electrical and spectroscopic measurements. The Monte Carlo model describes the movement of the fast electrons as particles, while in the fluid model, the slow electrons and positive ions are treated as a continuum. The transient continuity equations are solved together with the Poisson equation in order to obtain a self-consistent electric field. The source terms of the continuity equations and the electron multiplication coefficient (used for the determination of the secondary electron emission coefficient) are obtained from the Monte Carlo simulation. These two models are run iteratively until convergence is reached. Typical results are, among others, the charged particles densities, the fluxes, the electric field and potential distribution. It is found that the influence of the bottom of the cylindrical hollow cathode cannot be neglected. A very good agreement between calculations and experimental data was obtained. © 2002 Elsevier Science B.V. All rights reserved.

Keywords: Direct current; Hollow cathode discharge; Ar; Cu; Monte Carlo-fluid modeling; Discharge characteristics

1. Introduction

Hollow cathode discharges (HCD) are used in a wide variety of applications, for example in plasma processing (ion etching, thin film deposition, surface treatment) [1], in ion gas lasers [2,3], and in spectroscopic analysis, where the hollow cathode is used as an emission source, allowing direct excitation and analysis of samples and as a light source in absorption spectrometry because of its sharp and intense spectral lines [4–8].

This kind of glow discharge, which was first studied by Paschen [9,10], comprises two regions:

a dark space adjacent to the cathode surface, where the electric field is strong, which is called the cathode dark space (CDS) or sheath, and a rather luminous part beyond it, where the field is weak and which is called the negative glow region (NG) or plasma region. The cathode can be built in different shapes, for example as a spherical segment or as a pair of plane parallel plates or as a hollow cylinder. The anode (or anodes) is usually placed close to the cathode surface at such a distance that no positive column can be formed and that the NG can be confined inside the discharge cavity.

The operating voltage of the HCD is lower than in a glow discharge with single planar cathode for the same current density. Moreover, the voltage–

* Corresponding author. Fax: +32-3-820-23-76.

E-mail address: baguer@uia.ua.ac.be (N. Baguer).

current dependence shows two different regions: one with a steep slope at low current and the other with a smaller slope at higher current. The most specific characteristic of the HCD is the so-called hollow cathode effect [11], i.e. a large increase in the current density and light intensity, which is observed when the distance between the opposite cathode surfaces and the gas pressure are set in a way that the NG regions from facing cathode surfaces overlap. These properties are mostly due to the very efficient use of the fast electrons and ions in the HCD [12–14]. Indeed, most of the ions, which usually get lost at the boundaries of the NG with the anode and with the surrounding walls in the case of a plane cathode, can reach the surface of the cathode and release more electrons. The loss of fast electrons is also considerably reduced: the fast electrons can oscillate between opposite cathode surfaces ('pendulum effect') [14,15], using all their energy for excitation and ionization of the gas atoms. Some of these electrons can penetrate into the dark space opposite to the cathode of their origin and cause ionization collisions there. The new electrons thus created will be accelerated in the high CDS field and they generate new electrons, giving rise to an enhanced ionization rate in the CDS as well as in the NG.

Conventional HCDs usually operate at pressures up to 1.3 kPa, with a cathode voltage ranging from 200 to 500 V and a discharge current from a few mA up to 1 A [4,5,16].

In this paper, we will present our results for a cylindrical HCD obtained by a self-consistent numerical simulation and by measurements of the current–voltage dependence and the light emission intensity of some ArI spectral lines. Most studies, i.e. analytical models, experiments or mathematical simulations dealing with cylindrical HCDs are focused only on the radial properties of the discharge, assuming a hollow cathode of infinite length, and hence, a discharge uniform in the axial direction [17–23]. Here we intend to simulate the cylindrical geometry of a HCD as realistically as possible by taking into account the effect of the bottom of the hollow cathode in the discharge behavior. We investigate how the light emission intensities, the rates, densities, potential profiles

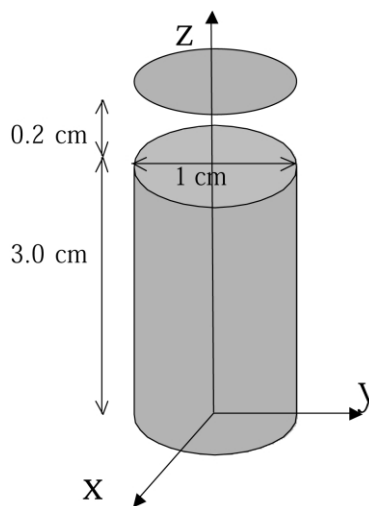


Fig. 1. Schematic picture of the cell geometry used in the model and in the experiments.

and the electron energy distribution change with varying discharge conditions.

2. Geometry and discharge conditions

The discharge geometry consists of a cylindrical cathode closed at one end and a disc anode at the other end, separated by 0.2 cm (Fig. 1). In a classical HCD, the length of the cylinder is typically 5–10 times larger than the radius in order to reduce the loss of electrons through the open end of the cylinder. We assumed a length of 3 cm and a radius of 0.5 cm.

The discharge conditions assumed in the model were taken from the experiments, i.e. the gas pressure was varied from 40 to 133 Pa, the discharge current ranged from 1 to 10 mA and a discharge voltage between 240 and 300 V was applied to the cathode, whereas the anode was grounded. The gas temperature was assumed to be at room temperature.

3. Experimental set up

The cylindrical HCD with the same dimensions as in Fig. 1 was placed in a Pyrex envelope. Both anode and cathode were made of high purity copper, and high purity argon was used as the

discharge gas. The discharge was operated in d.c. mode and digital multimeters measured the discharge current and the voltage. The background pressure of the vacuum system was approximately 1.33×10^{-4} Pa.

The spatial distribution of the light emission intensity in the discharge was scanned in the radial direction. For this aim, a 0.05-cm slit was machined into the anode disc along its diameter and the discharge tube was mounted on a precision translator equipped with a stepping motor driven by a PC. A 10-cm focal length quartz lens imaged the light of the discharge onto the entrance slit of a monochromator. A diaphragm was placed in front of the lens to obtain sufficient spatial resolution. For the recording of the spectral lines a photomultiplier tube (PMT) type EMI 9558B was used. The digitized signal of the PMT was sent to the PC, using an IEEE488 interface. The PC also controlled the wavelength positioning of the monochromator when recording the spectral scans.

4. Numerical model

The hybrid model presented here is a combination of two models: a Monte Carlo and a fluid model [24–31]. In the CDS, the condition for equilibrium approach is not fulfilled for electrons due to the high electric field and the large field variation over the electron mean free path. Indeed the energy gained by electrons from the field is not locally balanced by the energy lost through collisions; hence a flux of high-energy electrons will enter the NG, producing inelastic collisions. For these high-energy electrons a microscopic model based on a three-dimensional Monte Carlo method is used in the entire discharge (sheath and plasma region). The slow electrons in the NG and the positive ions in the whole discharge are treated with a classical equilibrium approach, i.e. the fluid model for collision dominated plasmas. For that, the following conditions should be fulfilled [32]: $\lambda \gg \lambda_c$ and $\tau \gg \tau_c$, i.e. the characteristic length (λ) and the time (τ) over which the plasma quantities change considerably, should be much larger than the mean free path (λ_c) and the collision time (τ_c).

4.1. Assumptions of the model

1. The discharge gas is assumed to be argon at room temperature and uniform throughout the discharge.
2. The species assumed to be present in the plasma are: neutral ground state Ar atoms, positive ions (Ar^+), slow electrons and fast electrons. Sputtered atoms and ions are not yet incorporated, since it was calculated in previous models for glow discharges, that they don't play a significant role in determining the electrical characteristics [33]. We plan in the near future to incorporate these species in our model, so that we can obtain a better feeling about the importance of these species in the model for HCD.
3. The processes taken into account are: ion induced secondary electron emission from the cathode sidewalls and bottom; electron impact excitation; and ionization and elastic collision with ground state Ar atoms. Recombination between the positive Ar ions and electrons can be neglected at our working pressure of 133 Pa or less (see below).
4. In order to obtain a better understanding of the HCD, the model should be developed at least in two directions:
 - The direction perpendicular to the cathode sidewalls, i.e. the radial direction, where the pendulum effect occurs.
 - The direction parallel to the cathode sidewalls, i.e. the longitudinal direction, in which the external discharge current will flow because of the position of the anode at the open end of the cathode (Fig. 1).

4.2. Description of the sub-models

4.2.1. Monte Carlo model

The Monte Carlo model simulates the trajectories and collisions of electrons emitted by the cathode and the ones created within the discharge gap by ionization [34–38]. The electrons move under the influence of a spatially dependent electric field through a gas of neutral atoms, assumed to be at rest in comparison with the high speed of

the electrons. The position where the secondary electrons are ejected from the cathode walls is determined based on the distribution of the ion flux to the walls (obtained from the fluid model; see below). The electrons are assumed to be emitted in the forward direction with an initial energy of 4 eV [38].

In each time step, the trajectory of the electron is calculated according to Newton's law:

$$X = X_0 + V_{0x}\Delta t - \frac{1}{2m}E_{fr}\cos\alpha\Delta t^2 \quad (1)$$

$$Y = Y_0 + V_{0y}\Delta t - \frac{1}{2m}E_{fr}\sin\alpha\Delta t^2 \quad (2)$$

$$Z = Z_0 + V_{0z}\Delta t - \frac{1}{2m}E_{fz}\Delta t^2 \quad (3)$$

$$V_x = V_{0x} - \frac{1}{m}E_{fr}\cos\alpha\Delta t \quad (4)$$

$$V_y = V_{0y} - \frac{1}{m}E_{fr}\sin\alpha\Delta t \quad (5)$$

$$V_z = V_{0z} - \frac{1}{m}E_{fz}\Delta t \quad (6)$$

where E_{fz} and E_{fr} are the axial and radial electric field, α is the azimuthal angle of the radial position, m is the electron mass, Δt is the time interval and X , Y , Z (V_x , V_y , V_z) and X_0 , Y_0 , Z_0 (V_{0x} , V_{0y} , V_{0z}), are the positions (velocities) after and before Δt , respectively.

The probability of collision during the time step Δt is calculated by: $P = 1 - \exp[-n\sigma_t(\varepsilon)\Delta s]$, where n is the gas density, σ_t is the total collision cross section and Δs is the distance traveled during the interval Δt . The cross-sections for the collisions taken into account (i.e. electron impact ionization, excitation and elastic collisions) are obtained from Phelps [39]. This calculated probability is compared with a random number (m), uniformly distributed in the interval between 0 and 1. If $m < P$, a collision occurs. To determine the kind of collision a second m is generated and compared with the relative probability of each collision. After each collision, the electron energy is calculated depending on the type of the collision. The new direction is determined by anisotropic scattering.

The scattering angle χ and the azimuthal angle of scattering ϕ are calculated using two m and the differential angular cross section $\sigma(\varepsilon, \chi)$ in the same way as described in Bogaerts et al. [38]. However, a new scattering formula was used [40]. From these angles, the new axial and azimuthal velocity angles are found by transformation of the coordinate frame of reference [35]. This procedure is repeated, until the electrons collide at the anode, where they can be absorbed, reflected or produce secondary electron emission, or until the electrons are transferred to the slow group. Indeed, when the energy of the fast electrons drops below the energy of the first excitation level of the Ar atoms, they are transferred to the slow-electron group. This threshold is selected so that only the fast electrons are capable of inelastic collisions [31].

4.2.2. Fluid model

In the fluid model, the transport of charged particles is represented by the continuity equations for ions and slow electrons [Eqs. (7) and (8), respectively] and by the momentum transfer equations for ions and slow electrons [Eqs. (9) and (10), respectively]. In order to obtain a self-consistent electric field, these equations are coupled with the Poisson equation [Eq. (11)]. Because of the cylindrical symmetry of our discharge cell, the fluid model is developed in cylindrical coordinates.

$$\frac{\partial n_i}{\partial t} + \vec{\nabla} \cdot \vec{j}_i = S_i \quad (7)$$

Continuity equation for ions

$$\frac{\delta n_e}{\delta t} + \vec{\nabla} \cdot \vec{j} = S_{\text{slow}} \quad (8)$$

Continuity equation for slow electrons

$$\vec{j}_i = -n_i\mu_i\vec{\nabla}V - D_i\vec{\nabla}n_i \quad (9)$$

Flux equation for ions

$$\vec{j}_e = n_e\mu_e\vec{\nabla}V - D_e\vec{\nabla}n_e \quad (10)$$

Flux equations for slow electrons

$$\nabla^2 V = -\frac{e}{\varepsilon_0}(n_i - n_e) \quad (11)$$

Poisson equation

S_i and S_{slow} are the source terms obtained as output from the Monte Carlo model, representing the number of ions and slow electrons created per unit volume and per unit time. D_i and D_e are the ion and electron diffusion coefficients, μ_i and μ_e are the ion and electron mobilities, n_i and n_e are the ion and slow electron densities, j_i and j_e are the ion and electron fluxes and V is the electric potential. The transport coefficients are taken from reference [26]. The fast electron density was not included in Poisson's equation because the fast electron density is much lower than the slow electron and ion densities [25,26].

The above set of equations is solved with the following boundary conditions:

- at the cathode: $V = -\text{Discharge voltage}$, $n_e = 0$, $\nabla n_i = 0$
- at the anode: $V = 0$, $n_e = 0$, $\nabla n_i = 0$

The system of equations is solved numerically following the procedure developed by Passchier and Goedheer [41,42].

4.3. Coupling of the models

The models are coupled as follows:

1. First the Monte Carlo model is run. In the first iteration, an initial electric field has to be proposed. Our initial assumption was a linearly decreasing electric field in most of the CDS and a constant electric field in the NG. At the 'cylinder corner', i.e. in the CDS belonging both to the cathode bottom and the cathode sidewalls, the electric field was assumed to have an axial and a radial component and each component was a function of the radial and the axial coordinates. The initial distribution of the ion flux bombarding the cathode was assumed to be uniform. This Monte Carlo model gives the source terms for the continuity equations in the fluid model and the electron multiplication coefficient which can be used to determine the secondary electron emission coefficient (γ) based on the condition of a self-sustained discharge (see below).
2. Secondly, the fluid model is run with the above source terms. It yields the electric field and the ion flux toward the cathode (j_{icath}). The new

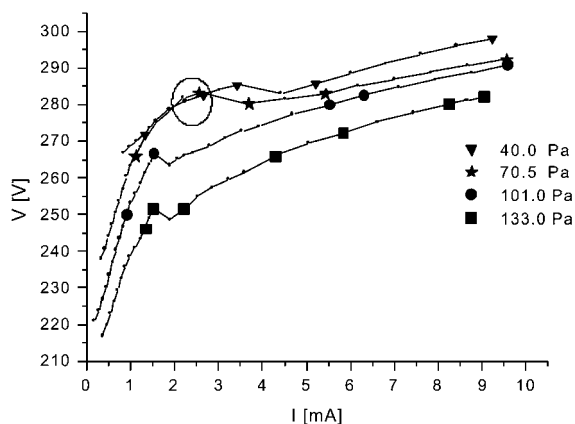


Fig. 2. Voltage–current dependence at different pressures. The lines with small points show the experimental measurements and the larger symbols represent the modeled discharge conditions. The spotlighted area shows the optimal discharge conditions for the occurrence of the hollow cathode effect.

flux of fast electrons leaving the cathode is calculated by $j_e = -\gamma j_{\text{icath}}$. These results will be used as input for the Monte Carlo model.

3. Third, with the obtained electric field and fast electron flux, the Monte Carlo model is run again.

Steps 2 and 3 are iterated, until convergence is reached (determined by the difference in the total current to the anode in two successive iterations being smaller than 1%). The total current to the cathode was not taken as a criterion of convergence, because it was already constant (to 10^{-2}) after a few iterations.

5. Results and discussion

5.1. Electrical conditions and emission intensities

The measured and calculated current–voltage dependence ($V-I$) in the pressure range from 40 to 133 Pa is presented in Fig. 2. For each pressure, approximately 20 $V-I$ points were measured. The symbols denote the conditions for which the calculations were performed (typically at 5–7 $V-I$ values per pressure). In the calculations, the total secondary electron emission coefficient, γ , was calculated in the Monte Carlo model based on the condition for the self-sustained discharge, under

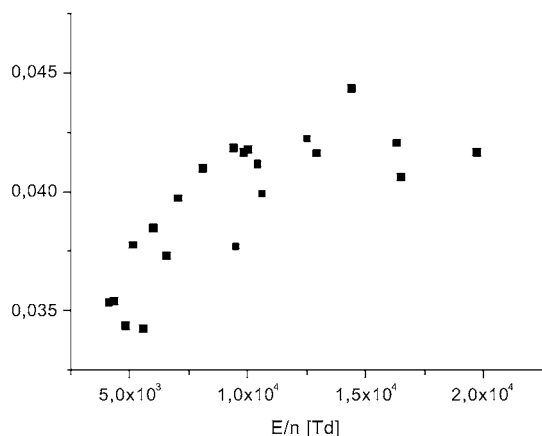


Fig. 3. Calculated secondary electron emission coefficient (γ) as a function of the reduced electric field (E/n).

the assumption that the ions were the main source of electron emission from the cathode, and that there is no recombination in the plasma or other volume losses, which is a correct approximation in our pressure range [12]. Then the condition for a self-sustained discharge can be written as: $\gamma = \frac{1}{M}$, where M is the so-called electron multiplication coefficient, defined as the amount of electrons created in the discharge per electron ejected from the cathode due to the ion induced secondary electron emission. In this way, γ was not used as a fitting parameter like in other work [30], but as a parameter really reflecting the amount of electron impact ionization in the discharge.

The obtained γ as a function of the reduced electric field at the cathode wall, i.e. the ratio of the electric field, (E) to the gas density (n) is shown in Fig. 3. Because the electric field is also a function of the axial position, we took as a representative value of the electric field at the cathode wall the value at $z = 1.5$ cm. The value of γ obtained here varies very little from 0.035 to 0.042, corresponding to a reduced electric field (E/n) from 5×10^3 to 2×10^4 Td, respectively. This value is in good agreement with the values obtained by Kruithof [43] for an Ar discharge in which the copper cathode was cleaned by sputtering without high temperature flashing, which is

also true in our case. With these values of γ , we obtained a good agreement between the experimental and calculated $V-I$ dependence. Hence, we can conclude that the assumption is justified, that in a HCD in this range of discharge conditions, the secondary electron emission by ions is the predominant process. In the review work of Phelps [39] it was suggested that in this range of E/n , the total secondary electron emission coefficient began to deviate from the ion-induced secondary electron emission coefficient. However, Phelps [39] deals with cold-cathode discharges in Ar in normal and abnormal glow modes, where it is expected that at $E/n > 10^4$ Td (which corresponds for this glow modes, at a discharge voltage greater than 500 V), the role of ionization by heavy particles becomes important, and then the total secondary electron yield increases, while the ion-induced secondary electron emission coefficient stays constant. The ionization by heavy particles begins to become important only for ion energies above 500 eV [44], which means that the discharge voltage should be at least 500 V. However, we are dealing with a cylindrical HCD in which the discharge voltage is clearly below 500 V (see Fig. 2). Hence, heavy particle ionization does not come into play. Although a cylindrical HCD is also a kind of glow discharge, it can, due to its distinguished properties, not be classified as a normal or an abnormal discharge, but it is classified as a conventional hollow cathode discharge [13]. It should be mentioned that in the conventional HCDs, the discharge voltage is lower than in a glow discharge for the same current density and pressure. Hence, the same value for E/n can be reached as in a glow discharge, at the same current density and pressure but at a lower voltage, so that heavy particle ionization is not yet important in this range of E/n for cylindrical HCDs.

The $V-I$ dependence of a HCD has two well-defined regions (see Fig. 2): one at low current density characterized by a steep slope and the other one, at higher current density with a smaller slope. For all the curves, a region of transition between the steep and the small slope was observed. Moreover, it appears also from Fig. 2 that the transition region is not continuous at certain points. This was experimentally checked

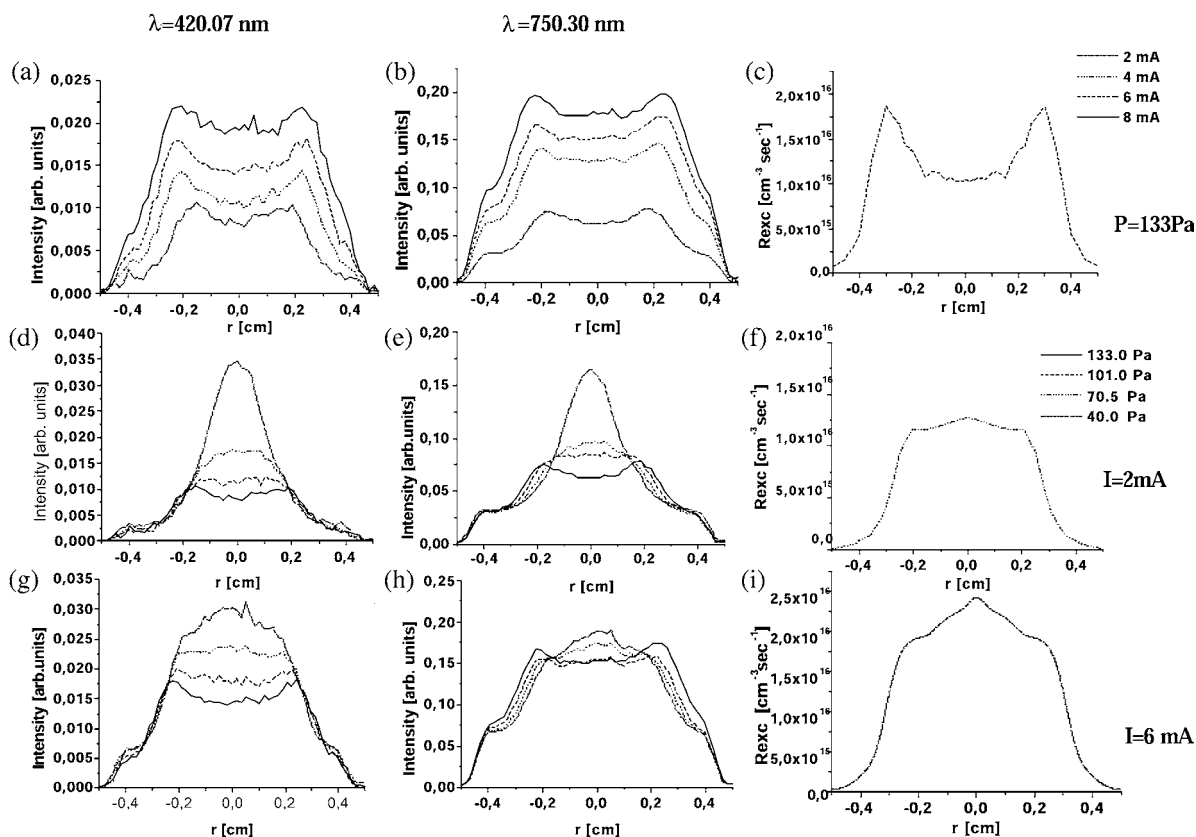


Fig. 4. Comparison of the radial profile of the recorded emission intensity for ArI 420.07 nm, ArI 750.30 nm and of the calculated electron impact excitation rate of the Ar atoms at $z = 1.5 \text{ cm}$, at constant pressure (133 Pa) for different currents (a, b and c), and at constant current for different pressures at $I = 2 \text{ mA}$ (d, e and f) and at $I = 6 \text{ mA}$ (g, h and i), respectively.

many times, to be sure that it was not a systematic error in the measurements. In fact, at these $V-I$ conditions of discontinuity, the light emission was most intense, i.e. it looks as if at these conditions the hollow cathode effect is optimal. Indeed at conditions where the light emission is most intense, the excitation processes are the most efficient [45]. This follows also from our simulation results. Indeed, it was found that for all pressures analyzed here, the average amount of excitation per electron emitted by the cathode (M_{exc}) was maximal at the $V(I)$ points corresponding to the transition region, which suggests the most intense light emission. Bearing in mind that the electron impact excitation is the main source of light in the NG [46], we have measured the spectral lines of ArI 420.07 nm, ArI 603.2 nm and

ArI 750.3 nm, which are mainly produced by electron impact excitation [45]. Fig. 4 shows the measured emission light intensities of some ArI lines (Fig. 4a,d,g for ArI 420 nm, and Fig. 4b,e,h for ArI 750.3 nm) and the calculated total electron impact excitation rate (Fig. 4c,f,i) as a function of radial position. It is clear that the results of the measurements and of the calculations show a similar shape and also behave similarly as a function of pressure and current.

In Arslanbekov et al. [13] and Kirichenko et al. [47], it was suggested that the optimal discharge condition (pressure, current and voltage) for the occurrence of the hollow cathode effect is reached when at constant voltage, the current increases with a decrease in pressure, or when at constant current, the discharge voltage drops with a

decrease in pressure. In order to check this, we plotted the current–pressure dependence (Fig. 5). It appears that in our discharge, this happens for a pressure between 40 and 70.5 Pa and for a current of approximately 2 mA (see also Fig. 2). Hence, at these conditions, the intensity of the spectral lines should be maximal, as can indeed be observed in the second and third row of Fig. 4, where the spectral line intensities and the calculated electron impact excitation rate obtained for discharge currents of 2 and 6 mA are plotted at different pressures. For both currents (2 and 6 mA) the maximum intensities of the spectral lines, as well as the maximum of the electron impact excitation rate, were obtained at a pressure of 40 Pa and the effect is most pronounced at the current of 2 mA. From Fig. 5, this effect is only visible at the discharge voltage of 282 V. It appears from Fig. 2 that the optimal condition for the hollow cathode effect occurs in the voltage range from 279 to 283 V (see spotlighted area). At the other voltages in the $I(P)$ dependence, the current decreases very slowly or stays constant with decreasing pressure, in the pressure range of 40–70.5 Pa. With further decreases in the pressure without increasing the voltage, the discharge current will drop until the discharge burns out.

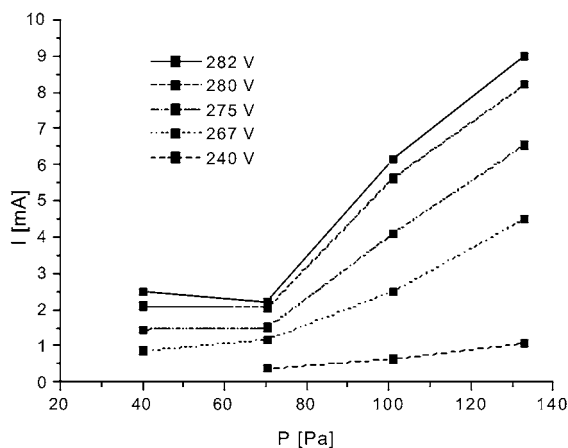


Fig. 5. Calculated and measured current–pressure dependence at constant voltage.

5.2. Calculated plasma quantities as a function of discharge conditions

In the following part, the influence of the current and pressure on the discharge behavior is analyzed in more detail. The calculated two-dimensional profiles of the electron impact ionization rate, electron density, potential distribution and axial electric field for different conditions are shown in Figs. 6–8. Figs. 6 and 7 illustrate the results at 133 Pa and a current of 9 and 1.4 mA, respectively, which correspond to the region of small and steep slope, respectively. Fig. 8 shows the results at 40 Pa and 9 mA (small slope). The thick black lines in the figures represent the cathode walls.

5.2.1. Electron collision rates

For all the conditions analyzed here, the absolute maximum of the electron impact ionization and excitation rates were observed near the bottom of the cathode cylinder in the NG region (Fig. 6a to Fig. 8a). This is a consequence of the strong axial and radial electric field in this region, which creates a flux of electrons with high energy in both directions. Hence, a large amount of ionization will occur, while in the rest of the discharge only the radial electric field remains strong. At a pressure of 133 Pa, the excitation and ionization rate profiles are more or less uniform in the axial direction along the discharge and they show a peak in the radial direction in the NG near the CDS–NG interface for all currents (see Fig. 6a, Fig. 7a). This can also be observed in Fig. 4, where the measured spectral lines intensities for ArI 420.07 nm, ArI 750.3 nm and the calculated electron impact excitation rates as a function of the radial distance at $z=1.5$ cm, are plotted for different currents at 133 Pa pressure (Fig. 4a–c). With decreasing current, the position of these peaks shifts toward the cylinder axis because the sheath length increases. Moreover, the absolute value of the rates decreases. With decreasing pressure, (compare Fig. 6a with Fig. 8a), the NG from the opposite sides of the cathode sidewalls start to collapse, and at 40 Pa, the collapse is completed, i.e. there are not two separate peaks at the two NG–CDS interfaces, but a common peak at the cylinder axis, corresponding to the best regime for

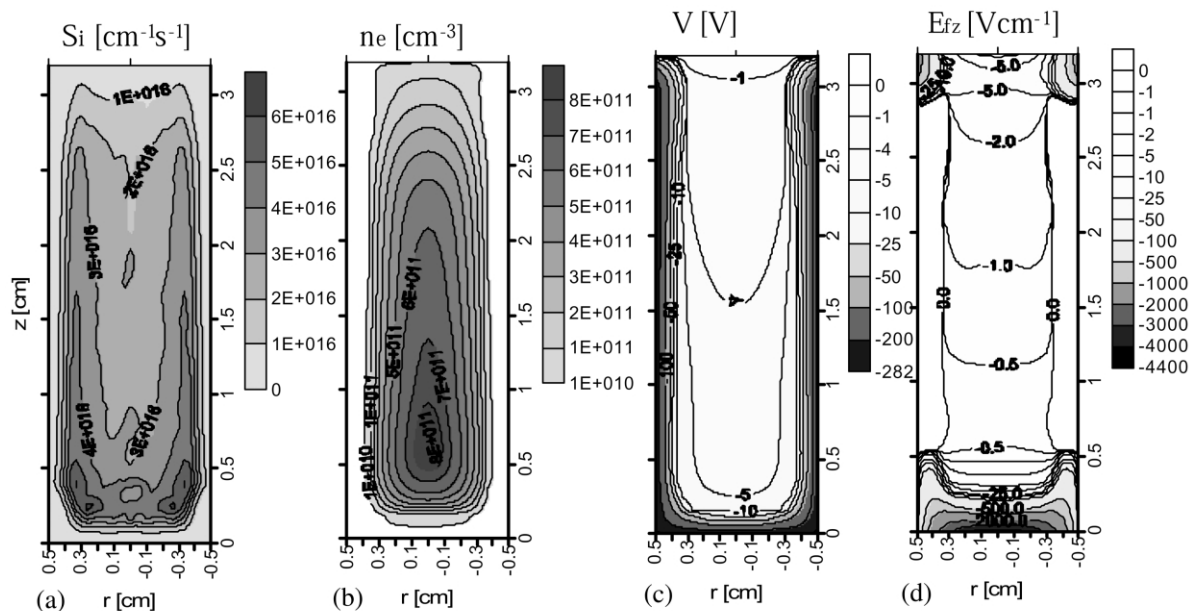


Fig. 6. Two-dimensional profile throughout the discharge at a pressure of 133 Pa and a current of 9 mA: (a) the electron impact ionization rate of the Ar atoms; (b) the slow electron density; (c) the potential distribution; and (d) the axial electric field.

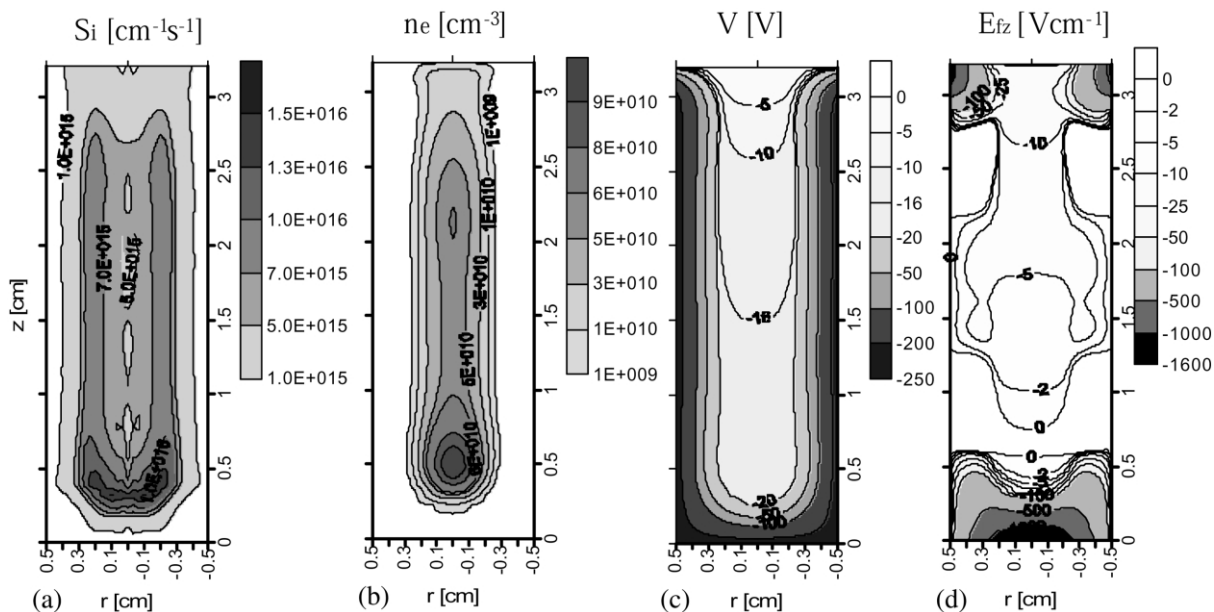


Fig. 7. Two-dimensional profile throughout the discharge at a pressure of 133 Pa and a current of 1.4 mA: (a) the electron impact ionization rate of the Ar atoms; (b) the slow electron density; (c) the potential distribution; and (d) the axial electric field.

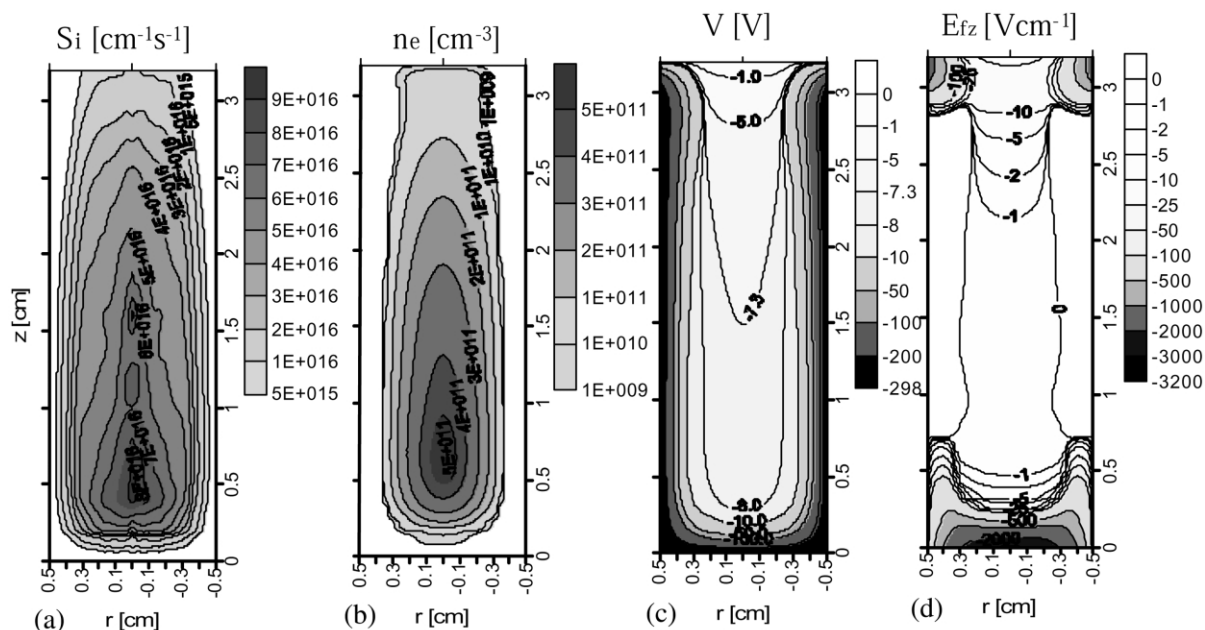


Fig. 8. Two-dimensional profile throughout the discharge at a pressure of 40 Pa and a current of 9 mA: (a) the electron impact ionization rate of the Ar atoms; (b) the slow electron density; (c) the potential distribution; and (d) the axial electric field.

the hollow cathode effect (HCE), as mentioned above (see also Fig. 4d–i).

The ionization processes inside the CDS were found to be important for all the conditions studied here, also at the currents corresponding to the region of the small slope in the V – I characteristic. This is in contrast to Arslanbekov et al. [13], who suggested, based on an analytical model, that for this region (small slope) the ionization processes in the CDS can be neglected. The amount of ionization inside the CDS increases with decreasing current, as the length of the CDS increases, and it is almost independent of the pressure. For example, at currents of approximately 10 mA it was found that 40% of the total ionization events occur inside the CDS, while for currents of approximately 1 mA, this value increases to 65%.

The rate at which the electrons are transferred to the slow group is zero in the sheath, where the electric field is strong and the electrons will remain fast, because they gain energy from the electric field. The maximum is reached in the beginning of the NG both in the axial and radial directions (not shown here).

5.2.2. Charged particle densities

The electron density in a HCD shows a tendency to decrease towards the open end of the cathode [5], as is shown in Fig. 6b, Fig. 7b and Fig. 8b. Similar to the electron impact ionization rate profiles, described above, it reaches its maximum in the lower part of the cathode cylinder, near the cathode bottom, but unlike the rates, this maximum is found at the cylinder axis for all the conditions, which is expected for the pressure values under consideration [5,23,48].

In almost the entire CDS, the slow electron density is zero (because of their high mobility), while the ion density is low and rather constant. This positive space charge region near the cathode walls yields the strong electric field in the CDS (see below).

Both densities begin to increase simultaneously at the end of the sheath. It is interesting to notice that the sheath region (indicated by the white region in the Fig. 6b, Fig. 7b and Fig. 8b) near the cathode bottom is shorter than at the cathode sidewalls, which will give rise to a higher axial electric field at the cathode bottom compared to

the radial electric field at the cylinder sidewall (see below). In the bulk plasma (or NG) the electron and ion density profiles are almost equal to each other, yielding a quasi-neutral region.

With decreasing current (compare Fig. 6b with Fig. 7b) the length of the sheath increases and the NG is more confined near the axis. Moreover, the maximum of the density profiles near the bottom is more pronounced and the density decreases faster toward the anode region, due to the increase of the loss of fast electrons to the anode. With the decrease in pressure (compare Fig. 6b with Fig. 8b), the profile of the densities in the axial direction show the same tendency as with the decrease in current as a consequence of the increasing loss of fast electrons to the anode (see also Fig. 12). Moreover, at the upper part of the cathode, near the anode, the sheath length increases compared with its lengths in the rest of the discharge cavity.

5.2.3. Electric potential

The electric potential distribution throughout the discharge is shown in Fig. 6c, Fig. 7c and Fig. 8c. The two characteristic regions of the HCD, i.e. the sheath and the bulk plasma can be clearly distinguished. In the sheath, the potential changes rapidly, for example, at 133 Pa (Fig. 6c), from -282 V at the cathode wall, to -10 V at the end of the sheath. The NG is characterized by a small potential gradient. It should be mentioned that this gradient increases with the drop in pressure and in current, as in the case of ion and electron densities.

At 133 Pa, the plasma potential was found equal to -4 V at the center of the discharge (Fig. 6c). With the decrease in current the plasma potential becomes more negative (e.g. -16 V at the center of the discharge at 1.4 mA and 133 Pa; see Fig. 7c). Moreover the value of the plasma potential at the CDS–NG interface also decreases (for $p=133$ Pa: from -10 V at $I=9$ mA to -20 V at $I=1.4$ mA). The same tendency was observed at other pressures and the effects were even more pronounced at low pressure. Indeed, at 40 Pa (Fig. 8c), the plasma potential at the discharge center at $I=9$ mA was found to be equal to -7 V and at $I=1.4$ mA, it was equal to -42 V. In Fig. 9 the value of the plasma potential at the discharge axis

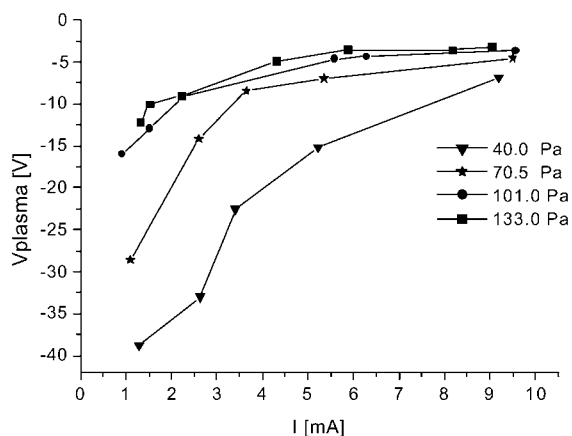


Fig. 9. Calculated plasma potential at the center of the discharge ($z=1.5$ cm, $r=0$ cm) as a function of the electric current at several pressures.

and at $z=1.5$ cm is plotted against the discharge current for all the conditions studied here. It is important to realize that for a cylindrical HCD the plasma potential was found to be negative throughout the entire discharge. However, this is not the case for all kinds of HCDs, see for example [29,30], where segmented HCD and HCD with planar cathodes were modeled, a positive plasma potential was found. We think that this difference is mainly due to the cathode geometry, i.e. in a cylindrical HCD, the loss of fast electrons and ions to the anode and to the wall is lower for the same conditions than in the segmented HCD or a one with planar cathodes. Hence, in a cylindrical HCD there is no need for the plasma potential to be positive in order to guarantee the current balance as is the case for example in the abnormal glow discharges with planar electrodes where the electric potential in the NG is characterized by a positive value [25,27]. Also, in Arslanbekov et al. [13], it is mentioned that the fraction of ions that get to the cathode to produce electrons by secondary emission in the modified HCD (segmented, for example) is similar to the abnormal GD and they considered modified HCD in that way as a discharge between abnormal GD and conventional (cylindrical) HCD.

In our experimental work, we were not able to measure the potential inside the discharge. How-

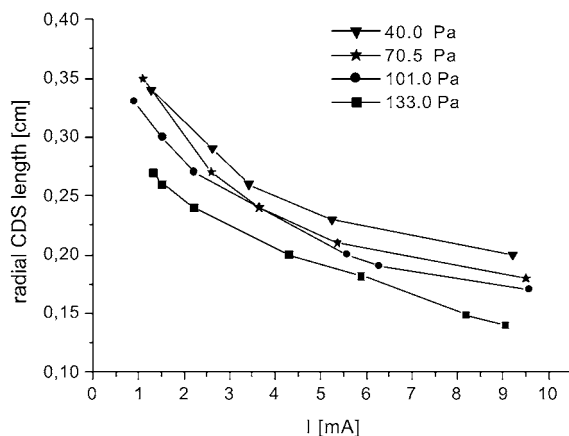


Fig. 10. Calculated radial CDS length at $z=1.5$ cm as a function of the total current at several pressures.

ever, in Kirichenko et al. [47], a negative plasma potential up to -30 V has been measured in a cylindrical HC discharges for Ar, Ne and He with cathode materials of Ni, Fe and Mo in a pressure range of 1.33–1330 Pa and currents from 30 to 200 mA. Also, Pfau et al. [49] have reported a negative plasma potential for a He–Ni cylindrical HCD in a pressure range of 100–500 Pa and currents from 2 to 6 mA.

5.2.4. Electric field

As can be deduced from the potential distribution, the electric field at the corner of the cylinder bottom is weaker compared to the field at the sidewall and bottom center. In Fig. 6d, Fig. 7d and Fig. 8d the axial electric field profiles are presented. Since the length of the sheath is defined here as the distance where the electric field gradient becomes very small in comparison with the field gradient inside the sheath, it is clear from these figures that the sheath length increases with decreasing current (Fig. 6d and Fig. 7d) and with decreasing pressure (Fig. 6d and Fig. 8d and also Fig. 10).

The radial electric field is the predominant one in most of the discharge cavity (except at the cathode bottom and at the anode region) and it depends strongly on the radial distance, while it is almost uniform in the axial direction. In the NG, the radial electric field changes slightly in the

radial direction (not shown). Kazantsev et al. [50] have also found the presence of a weak radial electric field in the NG of a HCD, by means of polarization spectroscopy.

The axial electric field is strong at the cathode bottom, especially at the center, where it is a strong function of the axial distance. In the NG, the axial electric field changes only a few V/cm in the entire NG. For example, at $p=133$ Pa and $I=9$ mA it changes from 0 to -10 V/cm. This is in good agreement with the measurement of the axial electric field in the NG of a HCD carried out by Helm [17]. With decreasing pressure and current, the gradient in the axial direction increases, e.g. the axial electric field changes from -5 V/cm at the bottom CDS–NG interface to -50 V/cm at the cathode end at $p=40$ Pa and $I=1.4$ mA (not shown here).

At the cathode bottom ‘corners’ and in the anode region, the axial and radial electric field shows a strong dependence of the radial as well as of the axial distance.

5.3. Influence of the bottom and top of the hollow cylinder

5.3.1. Cathode bottom

In some models, it is assumed that the influence of the cathode bottom of the HCD is negligible. In order to test this approximation, we study the effect of the emission of electrons from the cathode bottom on the discharge behavior, by comparing simulation results with and without emission from the bottom of the cylinder cathode. When the electron emission from the bottom is not taken into account, the maxima of the ionization rate (i.e. ion source term) profiles are shifted in the axial direction toward the center of the HCD. Hence, the maximum in the electron and ion density profiles, the maximum in the radial electric field and in the radial ion current density are also shifted in the axial direction toward the HCD center. When the electron emission from the cathode bottom is considered, all the maxima are found near the bottom of the HCD (as was shown in Figs. 6–8). Indeed, as a consequence of the strong axial and radial electric field near the bottom, a flux of high-energy electrons is created in both

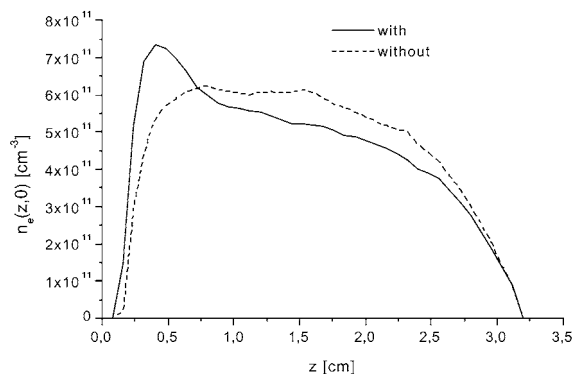


Fig. 11. Comparison of the calculated axial slow electron density profile at the discharge axis with and without taking into account secondary electron emission from the cathode bottom.

directions, increasing the number of electron impact ionization collisions, leading also to a maximum in the charged particle densities near the cathode bottom. We think that the special sputter and redeposition profiles observed at the bottom of the HCD ‘cylinder corners’ is also a consequence of the presence of the strong axial and radial electric field there and of the fact that secondary electron emission takes place not only at the axial wall, but also at the bottom wall.

In Fig. 11, the electron density profile at the discharge axis is shown with and without taking into account secondary electron emission from the cathode bottom. It is interesting to mention that when the cathode bottom emission is not considered, the potential distribution in the NG becomes slightly positive in the upper half of the HC, whereas when considering the cathode bottom emission, it remains negative in the entire discharge volume (see Fig. 6c, Fig. 7c and Fig. 8c).

The discharge characteristics in the radial direction, on the other hand, do not change considerably with or without taking into account cathode bottom emission, as is expected.

5.3.2. Anode

Fig. 12 shows the fraction of fast electrons reaching the anode, as a function of voltage at four different pressures. At all conditions investigated, this fraction is in the range of 1–6%. Hence, only a minority of the fast electrons gets lost at

the anode. This fraction increases slightly at decreasing pressure, voltage and current, explaining why the axial profile of the ionization rate, and consequently, the charged particle densities decreases toward the anode, as was mentioned above. When a fast electron reaches the anode, it can induce the emission of a new electron, or it can be reflected or absorbed by the anode wall, depending on its energy. Most of the fast electrons that reach the anode are absorbed, i.e. between 80 and 90%.

6. Summary and conclusions

A cylindrical hollow cathode glow discharge was studied experimentally as well as by means of a hybrid model. The hybrid model was based on the coupling of a Monte Carlo model for fast electrons (which gives the source terms of the continuity equations and the γ coefficient) and a fluid model for the slow electrons and ions (in which these continuity equations are solved together with the Poisson equation in order to obtain a self-consistent electric field). The model, as well as the experiments, were performed in a d.c.

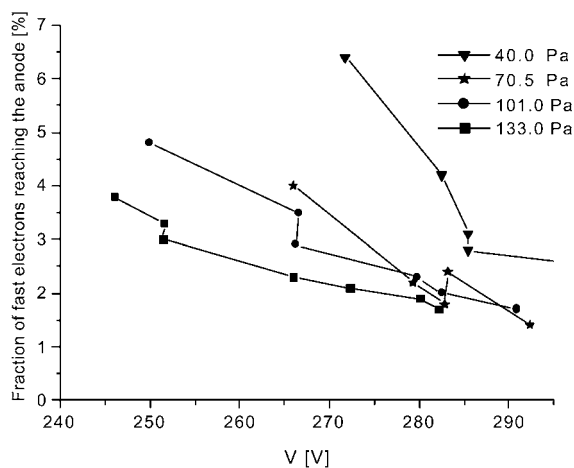


Fig. 12. Calculated fraction of fast electrons reaching the anode as a function of discharge voltage at several pressures.

cylindrical HCD with Ar as filling gas, in a pressure range from 40 to 133 Pa and a current varying from 1 to 10 mA; the anode and the cathode were made both of copper.

Summarizing our results, we can point out the following: the γ coefficient obtained was almost constant in the range of the reduced electric fields studied here, with a value of approximately 0.04, which agrees very well with reported data for a Cu cathode cleaned by sputtering without flashing. Moreover, it confirms our assumption that at the conditions studied here the ions are the main source of electron emission from the cathode and that the fundamental process of electron production is by ionization collisions of electrons with Ar atoms. The ionization collisions inside the CDS were found to be important for all conditions investigated, even at high currents. The maximum in the profile of the collision rates, the charged particle densities, the potential and electric field was found near the cathode bottom of the HCD cylinder. The plasma potential was found to be negative for all the discharge conditions investigated. When the emission from the cathode bottom was not considered, the maxima in the profiles were axially shifted to the cylinder center and the plasma potential was found positive at the upper half of the cylinder cathode. This shows the importance of considering the cathode bottom in order to have a more realistic description of the discharge. The loss of fast electrons to the anode increases and also the plasma potential becomes more negative with the decrease in pressure and in current. The best regime for the hollow cathode effect to occur was obtained, when at constant voltage, the current increases with decreasing pressure, i.e. at pressures between 40 and 70.5 Pa and a current of 2 mA. These conditions are characterized in the experimental data by the most intense light emission, and in our calculations, when the maximum of the calculated total electron impact excitation rate is found at the cell axis, i.e. in the form of a disc shape instead of a ring shape.

Acknowledgments

N. Baguer is financially supported by a New Research Initiative of the University of Antwerp.

A. Bogaerts is indebted to the Flemish Fund for Scientific Research (FWO) for financial support. This research is also sponsored by NATO's Scientific Affairs Division in the framework of the Science for Peace Programme, by the EC Thematic Network on Glow Discharge Spectroscopy for Spectrochemical Analysis (SMT4-CT98-7517) and by the Federal Services for Scientific, Cultural and Technical Affairs of the Prime Minister's Office through IUAP IV (Conv. P4/10). The experimental studies have been carried out at the Research Institute for Solid State Physics and Optics, Budapest, Hungary. We would like to thank Z. Donko, K. Kutasi, P. Hartmann, G. Bano for their help in the measurements and especially Z. Donko for reading the manuscript and for the interesting and helpful discussions.

References

- [1] A. Goldamn, J. Amoroux, *Gases: Macroscopic Processes and Discharges*, Plenum Press, New York, 1983, p. 293.
- [2] D.C. Gerstenberger, R. Solanki, J.G. Collin, *Hollow cathode metal ion lasers*, *IEEE J. Quant. Electron.* 16 (1980) 820–834.
- [3] A. Peard, Z. Donko, K. Rozsa, L. Szalai, R.C. Tobin, *Comparison of Cu-II 781 nm lasers using high voltage hollow cathode and hollow anode-cathode discharges*, *IEEE J. Quant. Electron.* 30 (1994) 2157–2164.
- [4] P.J. Slevin, W.W. Harrison, *The hollow cathode discharge as a spectrochemical emission source*, *Appl. Spectr. Rev.* 10 (1975) 201–255.
- [5] S. Caroli, *The hollow cathode emission source: a survey of the past and a look into the future*, *Prog. Analyt. Atom. Spectrosc.* 6 (1983) 253–292.
- [6] X. Cai, J.C. Williams, *Pilot study of the analytical performance of the pulsed HCD emission source*, *Appl. Spectr.* 49 (1995) 891–899.
- [7] K. Gilmodinov, B. Radziuk, M. Sperling, B. Welz, K. Nagulin, *Spatial distribution of radiant intensity from primary sources for atomic absorption spectrometry. Part 1: HC Lamps*, *Appl. Spectr.* 49 (1995) 413–423.
- [8] C. Schepers, J.A.C. Broekaert, *The use of a hollow cathode glow discharge as an atomic emission spectrometric element specific detector for chlorine and bromine in gas chromatography*, *J. Anal. At. Spectrom.* 15 (2000) 61–65.
- [9] F. Paschen, *Bohrs Heliumlinien*, *Ann. d. Phys.* 50 (1916) 901–940.

- [10] F. Paschen, Die funkenspektren des Aluminiums Teil 2, *Ann. d. Phys.* 71 (1923) 537–561.
- [11] P.F. Little, A. von Engel, The hollow cathode effect and the theory of the glow discharge, *Proc. R. Soc. Lond. A* 224 (1954) 209–227.
- [12] V.I. Kolobov, L.D. Tsendin, Analytical model of the hollow cathode effect, *Plasma Sources Sci. Technol.* 4 (1995) 551–560.
- [13] R.R. Arslanbekov, A.A. Kudryavtsev, R.C. Tobin, On the hollow-cathode effect: conventional and modified geometry, *Plasma Sources Sci. Technol.* 7 (1998) 310–322.
- [14] H. Helm, Experimenteller Nachweis des Pendel-effektes in einer Zylindrischen niederdruck Hohlkathoden entladung in *Ar*, *Z. Naturf.* 27a (1972) 1812–1820.
- [15] A. Guntherschulze, Glimmentladung an Hohlkathoden, *Zeitschr. f. Phys.* 2 (1930) 49–54.
- [16] K. Rozsa, Hollow cathode discharge for gas lasers, *Z. Naturf.* 35a (1980) 649–664.
- [17] H. Helm, F. Howorka, M. Pahl, Über der fallraum in einer Zylindrischen Hohlkathode, *Z. Naturf.* 27a (1972) 1417–1425.
- [18] Y. Kagan, Rate of ionization and density of the electrons in a hollow cathode in He, *J. Phys. D: Appl. Phys.* 18 (1985) 1113–1123.
- [19] S. Hashiguchi, M. Hasikuni, Multi-electron temperature models for HCD, *Jpn. J. Appl. Phys.* 28 (1989) 699–708.
- [20] S. Bukvic, L.M. Labat, Contributions studies on HCD, *Phys. Scripta* 46 (1991) 57–62.
- [21] R.R. Arslanbekov, A.A. Kudryavtsev, I.A. Movchan, Slow electron distribution function in a cylindrical HCD, *Sov. Phys. Tech. Phys.* 37 (6) (1992) 620–624.
- [22] R.R. Arslanbekov, A.A. Kudryavtsev, I. Movchan, Spatial and energy distributions of fast electrons in discharges with a cylindrical hollow cathode, *Sov. Phys. Tech. Phys.* 37 (4) (1992) 395–398.
- [23] J.P. Martinez, J.C. Amare, A study of the dark-space ionization dynamics in a stationary cylindrical HCD, *J. Phys. D: Appl. Phys.* 31 (1998) 312–318.
- [24] A. Bogaerts, R. Gijbels, W. Goedheer, Hybrid Monte Carlo-fluid model of a dc glow discharge, *J. Appl. Phys.* 78 (1995) 2233–2241.
- [25] A. Bogaerts, R. Gijbels, Two-dimensional model of a dc glow discharge: description of the electrons, Ar ions and fast Ar atoms, *Anal. Chem.* 68 (1996) 2296–2303.
- [26] L.C. Pitchford, N. Ouadoudi, J.P. Boeuf, Triggered breakdown in low-pressure HCD (pseudospark), *J. Appl. Phys.* 78 (1995) 77–89.
- [27] J.P. Boeuf, L.C. Pitchford, Pseudospark discharge via computer simulation, *IEEE Trans. Plasma Sci.* 19 (1991) 286–296.
- [28] A. Fiala, L.C. Pitchford, J.P. Boeuf, Two-dimensional hybrid model of low pressure glow discharge, *Phys. Rev. E* 49 (1994) 5607–5622.
- [29] Z. Donko, Hybrid model of a rectangular HCD, *Phys. Rev. E* 57 (1998) 7126–7137.
- [30] K. Kutasi, Z. Donko, Hybrid model of a plane-parallel HCD, *J. Phys. D: Appl. Phys.* 33 (2000) 1081–1089.
- [31] M. Surendra, D.B. Graves, G.M. Jellum, Self-consistent model of a direct glow discharge: treatment of fast electrons, *Phys. Rev. A* 41 (1990) 1112–1125.
- [32] J.M. Boyd, J.J. Sanderson, *Plasma Dynamics*, Thomas Nelson Ltd, London, 1969, p. 52.
- [33] A. Bogaerts, R. Gijbels, Role of the sputtered Cu atoms and ions in a dc glow discharge: combined fluid and Monte Carlo model, *J. Appl. Phys.* 79 (1996) 1279–1286.
- [34] A. Tran Ngoc, E. Marode, P.C. Johnson, Monte Carlo simulation of electrons within the cathode fall of a glow discharge in He, *J. Phys. D* 10 (1977) 2317–2329.
- [35] J.P. Boeuf, E. Marode, A Monte Carlo analysis of an electron sward in a non-uniform field: the cathode region of a glow discharge in He, *J. Phys. D* 15 (1982) 2169–2187.
- [36] D.A. Doughty, E.A. Den Hartog, J.E. Lawler, Current balance at the surface of a cold cathode, *Phys. Rev. Lett.* 58 (1987) 2668–2671.
- [37] S. Hashiguchi, M. Hasikuni, Calculations for the distribution function of energetic electrons in a He HCD with Monte Carlo method, *Jpn. J. Appl. Phys. Part 21* 1 (1988) 1010–1016.
- [38] A. Bogaerts, M. van Straaten, R. Gijbels, Monte Carlo simulation of an analytical GD: motion of electrons, ions and fast neutrals in the CDS, *Spectrochim. Acta Part B* 50 (1995) 179–196.
- [39] A.V. Phelps, Z. Lj. Petrovich, Cold-cathode discharges and breakdown in Ar: surface and gas phase production of secondary electrons, *Plasma Sources Sci. Technol.* 8 (1999) R21–R44.
- [40] A. Okhrimovsky, Private communication.
- [41] D. Paschier, PhD Dissertation, University of Utrecht (1994).
- [42] D. Paschier, W.J. Goedheer, A two-dimensional fluid model for an Ar rf discharge, *J. Appl. Phys.* 74 (1993) 3744–3751.
- [43] A.A. Kruithof, F.M. Penning, Determination of the Townsend coefficient for pure Ar, *Physica* 3 (1936) 515–533.
- [44] A.V. Phelps, Cross section and swarm coefficients for N ions and neutrals in N₂ and Ar ions and neutrals in Ar for energies from 0.1eV to 10KeV, *J. Phys. Chem. Ref. Data* 20 (1991) 557–573.
- [45] A. Bogaerts, Z. Donko, K. Kutasi, G. Bano, N. Pinhao, M. Pinheiro, Comparison of calculated and measured optical emission intensities in a dc Ar–Cu glow discharge, *Spect. Acta* 655 (2000) 1465–1479.
- [46] D.J. Sturges, H.J. Oskam, HCD in Hydrogen and the nobles gases, *J. Appl. Phys.* 37 (1966) 2405–2412.
- [47] V.I. Kirichenko, V.M. Tkachenko, V.B. Tyutyunnik, Influence of dimensions, cathode material and gas on

- the optimum pressure for a cylindrical HCD, *Sov. Phys. Tech. Phys.* 21 (1976) 1080–1086.
- [48] F. Howorka, M. Pahl, Experimentelle bestimmung innerer und äußerer Parameter des negativen Glimmlichtplasmas einer Zylindrischen Hohlkathodenentladung in Ar, *Z. Naturf.* 27a (1972) 1425–1433.
- [49] S. Pfau, R. Kosakov, M. Otte, J. Rohmann, Experimental investigation of cylindrical HCD, *Proc. XXIV ICPIG*, Warsaw, 1999, p. 262.
- [50] S.A. Kazantsev, A.G. Petrashen, N.T. Polezhaeva, V.N. Rebane, Polarization spectroscopy of the ionic component of plasma, *Opt. Spectrosc.* 68 (1990) 740–743.